Catalysis Communications 68 (2015) 15–19

Contents lists available at ScienceDirect

Catalysis Communications

journal homepage: www.elsevier.com/locate/catcom

Short communication

Enhanced photocatalytic properties of a novel GO-Ag-$C_6H_5Ag_3O_7$ nanocomposite

Fenglin Liu [a], Xianjie Chen [a], Lihong Tian [a,b,*], Bing Liu [a], Qinghua Xia [a], Xiaobo Chen [b,**]

[a] Hubei Collaborative Innovation Center for Advanced Organochemical Materials, Ministry-of-Education Key Laboratory for the Synthesis and Applications of Organic Functional Molecules, Hubei University, Wuhan 430062, PR China
[b] Department of Chemistry, University of Missouri — Kansas City, Kansas City, MO 64110, USA

ARTICLE INFO

Article history:
Received 10 March 2015
Received in revised form 12 April 2015
Accepted 13 April 2015
Available online 21 April 2015

Keywords:
Graphene oxide
Silver citrate
Plasmonic photocatalyst
Nanocomposite

ABSTRACT

A novel graphene oxide-Ag-$C_6H_5Ag_3O_7$ nanocomposite was prepared by a facile precipitation reaction with the aid of photo-reduction. The rich surface functional groups of graphene oxide (GO) interacted with silver cations, provided the nucleation sites and induced the formation of $C_6H_5Ag_3O_7$ nanoparticles on the GO surface uniformly. The nanocomposite displayed an enhanced photocatalytic activity compared with pure $C_6H_5Ag_3O_7$ and GO under simulated sunlight, due to the reduced recombination of plasmon-induced electron–hole pairs on the Ag nanoparticles by the GO. This study likely provides one possibility of exploiting stable Ag/silver (I) complex photocatalysts in dealing with environmental contaminants.

© 2015 Elsevier B.V. All rights reserved.

1. Introduction

The photocatalytic oxidation technology utilizing solar energy has caught increasing interests in dealing with various environmental pollutants [1,2]. Some significant photocatalysts (e.g., TiO_2) can only respond to the ultraviolent (UV) light which only accounts for ca. 5% in sunlight. Therefore, exploiting efficient sunlight-triggered photocatalysts has a practical significance. Since Huang et al. reported an efficient and stable Ag/AgCl plasmonic photocatalyst under visible light, some Ag/silver (I) compounds plasmonic photocatalysts, AgX (X = Cl, Br, I) and Ag_3PO_4, have attracted considerable attention due to the strong surface plasmonic absorption of the Ag nanoparticles in visible light region and their excellently photocatalytic properties. Previous studies demonstrated that the AgX and Ag_3PO_4 surfaces were terminated with X^- and PO_4^{3-} groups of negative charges and those groups played an important role in attracting the holes from the plasmon-induced Ag nanoparticles, promoting the separation of electron–hole pairs and improving the activity of plasmonic photocatalysts [3–7]. This provides a reference for designing new Ag/silver (I) compounds plasmonic photocatalysts.

Silver (I) citrate complex is an environment-friendly material, mainly studied in the antibacterial field currently [8]. On silver citrate surface, there are some amounts of carboxylate groups with negative charges. Those groups are beneficial to attracting the holes from Ag nanoparticles and enhancing the photocatalytic activity of the Ag/silver citrate nanostructure under visible light irradiation. However, a thorny problem is that silver citrate tends to photo-decompose, inhibiting the application of silver citrate in dealing with the environmental problems. Therefore, it is important to prevent silver citrate from photodecomposing. Recently, many approaches, such as forming hetero-photocatalysts [9] and employing stabilizers [10], have been taken to improve the photostability of silver-containing compounds. Graphene oxide (GO) has been proven to be a promising candidate for enhancing the photocatalytic activity and photostability of silver-containing compounds, due to its unique conjugated structure, electronic property and high surface area [11–15].

Here, we report a novel graphene oxide-Ag-$C_6H_5Ag_3O_7$ (GO-Ag-$C_6H_5Ag_3O_7$) nanocomposite prepared by a facile precipitation reaction with the aid of photo-reduction. GO was employed to stabilize the Ag/$C_6H_5Ag_3O_7$ structure and prevent the citrate from photo-oxidation. The photocatalytic activity was investigated on the degradation of Rhodamine B (RhB) and methyl orange (MO) under simulated sunlight. The active species and photocatalytic mechanism were also studied in details.

2. Experimental section

2.1. Synthesis of GO-Ag-$C_6H_5Ag_3O_7$

All the reagents were obtained from Sinopharm Chemical Reagent Co., Ltd. and Alfa Aesar, and used without the further purification. GO was obtained by a modified Hummer's method (see the Supporting material) [16]. The GO-Ag-$C_6H_5Ag_3O_7$ nanocomposites were synthesized

* Correspondence to: L. Tian, Hubei Collaborative Innovation Center for Advanced Organochemical Materials, Ministry-of-Education Key Laboratory for the Synthesis and Applications of Organic Functional Molecules, Hubei University, Wuhan 430062, PR China.
** Corresponding author.
E-mail addresses: tian7978@hubu.edu.cn (L. Tian), chenxiaobo@umkc.edu (X. Chen).

http://dx.doi.org/10.1016/j.catcom.2015.04.022
1566-7367/© 2015 Elsevier B.V. All rights reserved.

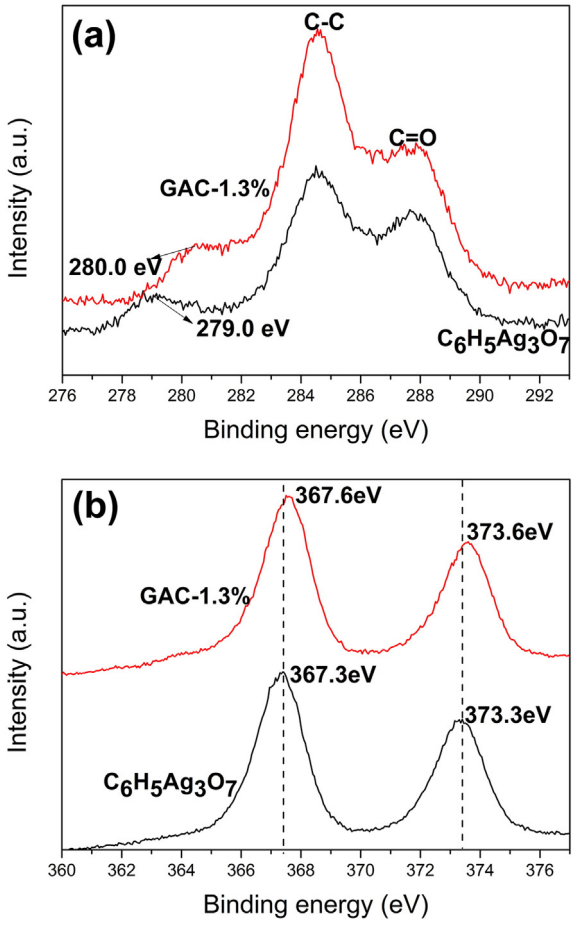

Fig. 1. A comparison of C 1s (a) and Ag 3d (b) XPS spectra of $C_6H_5Ag_3O_7$ and GAC-1.3%.

by a facile precipitation method with the aid of photo-reduction. Typically, a certain amount of GO dispersion was added to 6 mL $AgNO_3$ solution (0.1 M) to obtain a homogenous solution. Then, 20 mL ammonium citrate solution (0.1 M) was added dropwise under magnetic stirring at room temperature. The gray precipitation was collected by centrifugation and rinsed with deionized water. The precipitation was re-dispersed into 20 mL water and irradiated for 2 h. The obtained powders were dried in an oven at 70 °C for a day and denoted as GAC-wt.%, where wt.% is the weight ratio of GO to $C_6H_5Ag_3O_7$. Pure $C_6H_5Ag_3O_7$ was prepared under the same experimental conditions without GO.

2.2. Characterization

The crystalline structure of as-prepared samples was determined by X-ray powder diffraction (XRD, D/MAX-IIIC, Japan) with Cu Kα radiation ($\lambda = 1.54$ Å) at the scan rate of 5° min^{-1} with a step of 0.02°. Morphologies of samples were investigated by transmission electron microscopy (TEM, Tecnai G20). X-ray photoelectron spectroscopy (XPS) measurements of nanocomposites were carried out using a VG Multilab 2000 spectrometer with an AlKa X-ray source (Thermo Electron Corporation), and all the spectra were calibrated to the C 1s peak at 284.6 eV. UV–visible diffuse reflectance spectra (DRS) were achieved by dry-pressed disk samples on a UV–vis spectrophotometer (UV-3600) with $BaSO_4$ as the reference sample. Raman spectra were obtained by a laser micro-Raman spectrometer (Invia, Renishaw) with the excited wavelength at 514.5 nm. The surface organic groups of products were determined by Fourier transform infrared spectrometry (FT-IR, NICOLET IS10).

2.3. Evaluation of photocatalytic activity

The photocatalytic performance of materials was evaluated by degrading RhB using a 300 W high-pressure xenon lamp to simulate the sunlight (CEL-HXF300). In a typical experiment, 10 mg of photocatalyst was suspended in 40 mL of 10 $mg \cdot L^{-1}$ RhB aqueous solution. Before the irradiation, the suspension was dispersed by ultrasonic method for 30 min and magnetically stirred for 1 h in the dark to ensure the establishment of the adsorption/desorption equilibrium of RhB on the catalyst surface. Then the solution was placed in a quartz reaction vessel and bubbled with air under simulated sunlight irradiation. At given time intervals, 4 mL solution was taken out and the particles were removed by centrifuge. The concentration of RhB in the remained solution was monitored by colorimetry using a UV–vis spectrophotometer (UV-3600). The degradation of MO was conducted on the same condition to that of RhB.

3. Results and discussion

3.1. Crystalline structure

It can be seen in Fig. S1 that the diffraction peaks of the as-prepared white powders could be indexed to the monoclinic $C_6H_5Ag_3O_7$ (JCPDS, no. 01-0030) (see the Supporting information) (Fig. S1a). After photo-irradiation for 2 h, $C_6H_5Ag_3O_7$ partially photo-decomposed to produce some silver tartrate (JCPDS, no. 01-0441) and metallic silver (Fig. S1b). However, it was noted that the GAC-1.3% nanocomposite still displayed characteristic peaks of monoclinic $C_6H_5Ag_3O_7$ phase, and only weak peaks of metallic silver was observed after the irradiation for 2 h. This implied that the

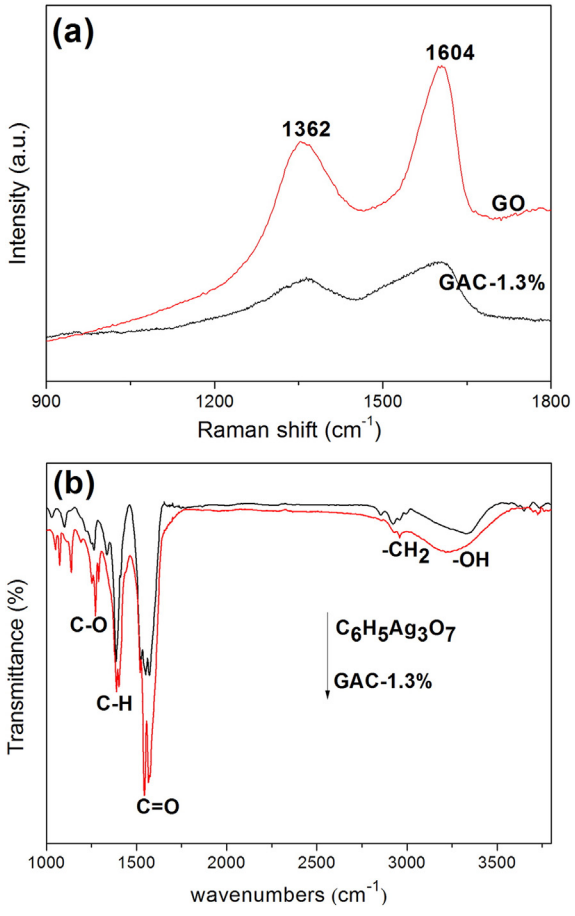

Fig. 2. Raman spectra (a) and FT-IR spectra (b) of $C_6H_5Ag_3O_7$ and GAC-1.3%.

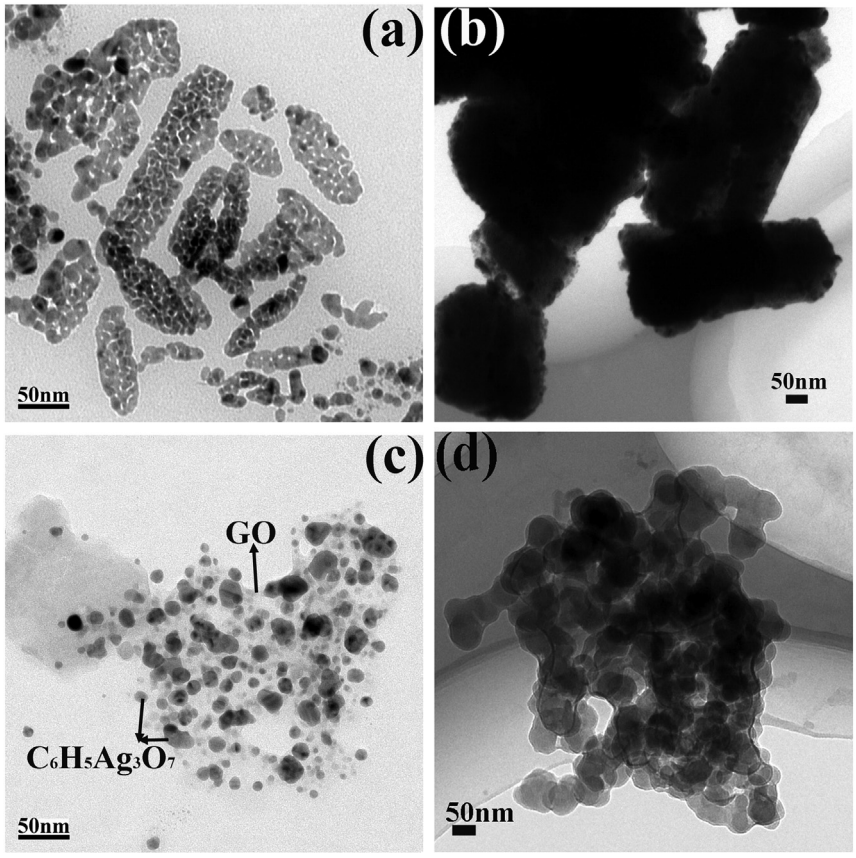

Fig. 3. TEM images of as-prepared $C_6H_5Ag_3O_7$ (a), GAC-0.6% (b), GAC-1.3% (c) and GAC-1.9% (d).

presence of GO inhibited the photodecomposition of $C_6H_5Ag_3O_7$ in the nanocomposite materials. Once the GO-inorganic nanocomposite was formed, the peaks attributed to GO became invisible, due to the low diffraction intensities of GO [17].

3.2. XPS spectra

XPS analysis was conducted to investigate the surface compositions and chemical states of the materials. Fig. 1(a) shows the C 1s XPS spectra of $C_6H_5Ag_3O_7$ and GAC-1.3% nanocomposites. For $C_6H_5Ag_3O_7$, the two peaks with electron binding energy at 284.6 eV and 288.0 eV were attributed to C–C and C═O groups resulting from the citrate. The peak at 279.0 eV was ascribed to Ag–O–C linkage [11]. Compared with the C 1s XPS spectra of $C_6H_5Ag_3O_7$, the two peaks attributed to C–C and C═O groups showed no change in GAC-1.3%. The distinct difference was that the peak of Ag–O–C linkage up-shifted to 280.0 eV. This indicated the presence of strong chemical interactions between GO and $C_6H_5Ag_3O_7$ in the nanocomposites. Ag 3d XPS spectra were shown in Fig. 1(b). The bands at 367.3 and 373.3 eV were attributed to Ag $3d_{5/2}$ and Ag $3d_{3/2}$ from the presence of Ag^+ in $C_6H_5Ag_3O_7$. For GAC-1.3% nanocomposite material, those bands shifted to higher binding energy. This suggested the chemical environment of oxygen of $C_6H_5Ag_3O_7$ in the nanocomposite was different from that in pure $C_6H_5Ag_3O_7$. The bands of metallic Ag^0 were invisible because of a low amount of Ag^0 in the nanocomposite.

3.3. Raman and FT-IR spectra

The GAC-1.3% composite material was further characterized by Raman spectra, as shown in Fig. 2a. The two prominent peaks (~ca. 1362 and 1604 cm^{-1}) in GO were assigned to the D band and the G band, respectively. The D band arose from the sp^3-hybridized carbon and structural defects, and the G band corresponded to the sp^2 carbon [18]. For GAC-1.3% nanocomposite, the positions of those Raman peaks from the GO showed no change. However, the intensity ratio, I_D/I_G, increased to 0.88 from 0.77 in pure GO. This indicated the removal of partial oxy-functional groups on GO to form an ordered crystal structure. That facilitated the charge transfer between GO and composite component [19].

FT-IR spectra of $C_6H_5Ag_3O_7$ and GAC-1.3% were compared in Fig. 2b. For $C_6H_5Ag_3O_7$, the weak absorption bands below 1000 cm^{-1} were assigned to different Ag–O bonds in $C_6H_5Ag_3O_7$ complex. The band located at 1264 cm^{-1} was ascribed to C–O stretching vibration, and the bands at 1383 and 2850–2959 cm^{-1} corresponded to C–H vibrations. The strong peak at 1570 cm^{-1} was attributed to the asymmetric C═O stretching of the carboxylate groups. The absorption bands of C–O and C═O in GAC-1.3% composite shifted to higher wavenumbers. This suggested that GO was successfully composited with $C_6H_5Ag_3O_7$ [20].

3.4. Morphology and tentative formation

Fig. 3 shows the typical TEM images of $C_6H_5Ag_3O_7$ and GAC composite materials. Before illumination (Fig. 3a), small $C_6H_5Ag_3O_7$ particles with the size of about 8 nm self-assembled into a porous structure, likely through an intramolecular hydrogen bond between the OH group and one of the terminal carboxylate groups [21]. After illumination for 2 h, the particles aggregated densely into the micro-sticks decorated with some Ag nanoparticles (see Supporting material Fig. S2). According to the XRD results, these micro-sticks were silver tartrate. However, GO could prevent the formation of silver tartrate micro-sticks from $C_6H_5Ag_3O_7$ particles. For the GAC-0.6% nanocomposite, some dense micro-sticks were still visible in Fig. 3b. When the amount of GO reached 1.3%, small silver citrate nanoplates with the size of 10–25 nm decorated on the surface of GO (Fig. 3c), indicating the presence of

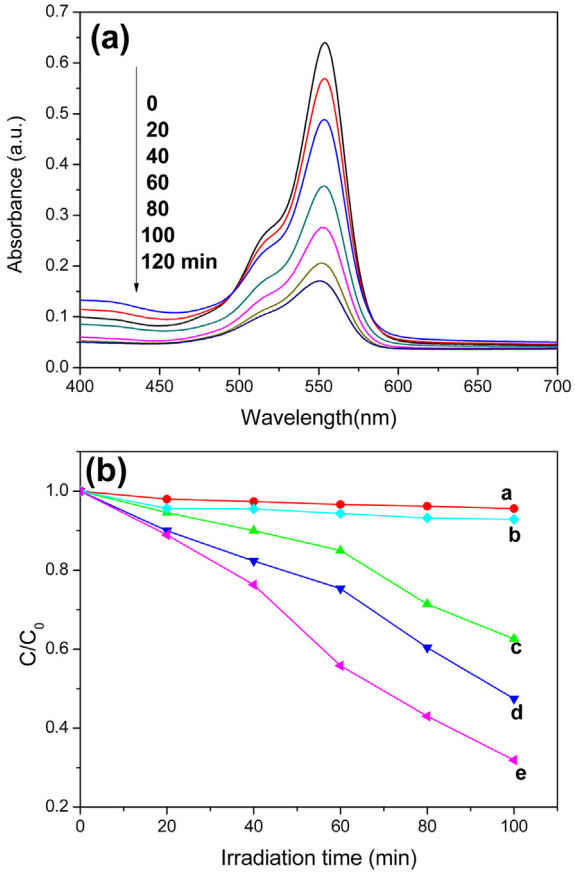

Fig. 4. (a) The degradation of RhB on GAC-1.3% under the simulated sunlight and (b) a comparison of photocatalytic activity of $C_6H_5Ag_3O_7$ and all GAC nanocomposites, a: $C_6H_5Ag_3O_7$, b:GO, c: GAC-0.6%, d: GAC-1.9%, and e: GAC-1.3%.

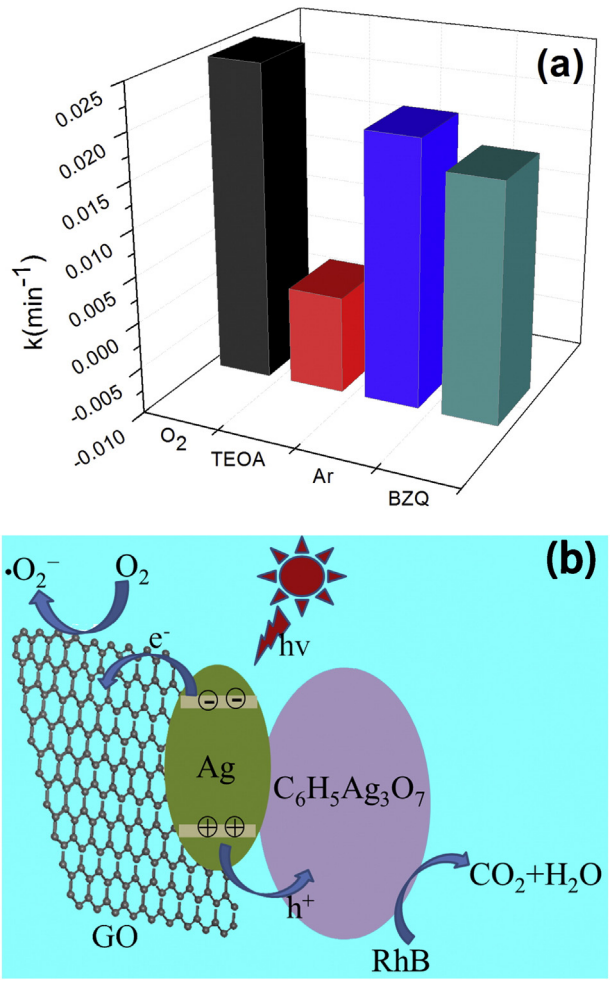

Fig. 5. (a) The degradation of RhB on GAC-1.3% nanocomposites in the presence of different scavengers and Ar-saturated conditions, and (b) proposed photocatalytic mechanism of GAC.

strong interaction between GO and Ag^+. Excess GO resulted in $C_6H_5Ag_3O_7$ particles embedded in the nanocomposite (Fig. 3d).

Based on the results of XPS and TEM, the tentative formation process of $C_6H_5Ag_3O_7$ and GAC composite was illustrated in the supporting material Scheme S1. $C_6H_5Ag_3O_7$ could be obtained easily from the coordination of Ag^+ with citrate at room temperature. These $C_6H_5Ag_3O_7$ nanoparticles self-assembled into porous structure due to intramolecular hydrogen bonding. After illumination, the compact silver tartrate micro-sticks formed. However, for GAC composite, rich functional groups (e.g., –OH, –COOH) on the GO surface interacted with Ag^+ to weaken the hydrogen bonding among the citrates, leading to the formation of uniform $C_6H_5Ag_3O_7$ nanoplates on the surface of GO (Fig. 3c).

3.5. Optical properties

The optical absorption properties of photocatalysts are important for their photocatalytic performance [22]. Fig. S3 (see the Supporting material) illustrates the UV–visible diffuse reflectance spectra of $C_6H_5Ag_3O_7$ and all GAC nanocomposites. In Fig. S3, pure $C_6H_5Ag_3O_7$ had an absorption merely in ultraviolent region. However, a broad and strong absorption was clearly detected in the UV and visible regions for all GAC nanocomposites. This indicated GAC nanocomposites could act as a sunlight-driven catalyst. The absorption at ~410 nm was attributed to the surface plasmon resonance (SPR) of Ag nanoparticles formed on the surface of nanocomposite. This suggested the presence of metallic Ag in composite catalysts [23,24]. In addition, GO resulted in a gradually enhanced SPR absorption in visible light region with the increase of GO content. Nevertheless, the excess GO (1.9%) hindered the absorption of Ag nanoparticles and led to a low absorbance at 410 nm for GAC-1.9%.

3.6. Photocatalytic activity and active species

The photocatalytic activity and stability of the as-prepared $C_6H_5Ag_3O_7$ and GAC nanocomposites were evaluated by the photodegradation of RhB in aqueous solution under simulated sunlight. As seen from Fig. 4b, both pure GO and $C_6H_5Ag_3O_7$ had no activity on the degradation of RhB. However, the maximum absorption of RhB at 554 nm decreased gradually on GAC nanocomposite during the irradiation (Fig. 4a). That revealed the significant degradation of RhB caused by the active oxygen species on GAC [25]. Moreover, the maximum absorption peak of RhB showed no shift during the degradation. This indicated that the decarboxylation of RhB did not occur with the self-photosensitization process [26].

Among all the GAC nanocomposites, the GAC-1.3% nanocomposite exhibited the highest photocatalytic activity on the degradation of RhB under simulated sunlight. After irradiation for 100 min, the degradation rate of RhB reached 70% on GAC-1.3%, whereas it dropped to 47% and 53% on GAC-0.6% and GAC-1.9%, respectively. This was likely due to the strongest plasmonic absorption of GAC-1.3% among all the GAC nanocomposites (DRS results). In addition, the photostability of GAC nanocomposites was investigated by recycling runs and exhibited in Supporting material Fig. S4. Clearly, GAC-1.3% was stable and kept an excellent activity on the degradation of RhB after 3 successive recycles. In addition, the degradation of MO, an anion dye, was also investigated on GAC nanocomposites (Fig. S5c, see the Supporting material). GAC nanocomposites had a relative low activity on the photocatalytic

degradation of MO compared with that of RhB. That was ascribed to the lower adsorption of MO (7.3%) than RhB (13.1%) on GAC nanocomposite (Supporting material Fig. S5a and b). The result indicated that GAC nanocomposites selectively absorbed and effectively degraded the cationic dye.

To explore the photocatalytic process of RhB on the GAC nanocomposite, a series of trapping experiments of active species were performed. Two different quenchers: p-benzoquinone (BZQ, a $^{\bullet}O_2^-$ radical scavenger) and triethanolamine (TEOA, a hole scavenger), were used in the photocatalytic reaction. RhB was also been decomposed in argon atmosphere to investigate the role of O_2. Obviously, holes were the main active species on the direct degradation of RhB (Fig. 5a). In addition, $^{\bullet}O_2^-$ radicals also made a contribution to the degradation of RhB. Based on the above experimental results, tentative photocatalytic mechanism of GAC nanocomposites was proposed in Fig. 5b. Ag nanoparticles were plasmon-excited and produced a large number of electron–hole pairs. GO acted as an electron acceptor to prevent the recombination of electrons and holes under simulated sunlight irradiation. Then, electrons accumulating on GO reacted with O_2 and produced active $^{\bullet}O_2^-$ radicals. The holes transferred to the surface of $C_6H_5Ag_3O_7$ and oxidized RhB molecules directly. The strong interaction between GO and $C_6H_5Ag_3O_7$ prevented the oxidation of citrate and sustained the photostability of the GAC nanocomposite. That resulted in an active and stable photocatalytic activity.

4. Conclusions

In conclusion, a novel GO-Ag-$C_6H_5Ag_3O_7$ nanocomposite has been successfully prepared by a simple precipitation method with the aid of photo-reduction. It exhibits a high plasmon-photocatalytic activity on the degradation of organic dye RhB than pure GO and $C_6H_5Ag_3O_7$ under simulated sunlight. The high photocatalytic activity is due to the inhibition of the recombination of plasmon-induced electron–hole pairs by the GO and the strong adsorption of cationic dye on nanocomposite. The holes and $^{\bullet}O_2^-$ radicals are the main active species on the photocatalytic oxidation of organic contaminants. The interaction between GO and $C_6H_5Ag_3O_7$ prevents the photo-oxidation of citrate and stabilizes the GO-Ag-$C_6H_5Ag_3O_7$ nanocomposite. After three recycling runs, GAC-1.3% still keeps a high activity on the degradation of RhB.

Acknowledgments

We gratefully acknowledge the support from National Natural Science Foundation of China (No. 51302072), Natural Science Foundation of Hubei Provincial Department of Education (No. Q20131010), and Natural Science Fund for Creative Research Groups of Hubei Province of China (No. 2014CFA015). X. C. thanks the support from College of Arts and Sciences, University of Missouri — Kansas City and the University of Missouri Research Board.

Appendix A. Supplementary data

Supplementary data to this article can be found online at http://dx.doi.org/10.1016/j.catcom.2015.04.022.

References

[1] C. Chen, W. Ma, J. Zhao, Chem. Soc. Rev. 39 (2010) 4206–4219.
[2] J. Zhang, Q. Xu, Z. Feng, M. Li, C. Li, Angew. Chem. Int. Ed. 47 (2008) 1766–1769.
[3] P. Wang, B. Huang, X. Zhang, X. Qin, H. Jin, Y. Dai, Z. Wang, J. Wei, J. Zhan, S. Wang, J. Wang, M.H. Whangbo, Chem. Eur. J. 15 (2009) 1821–1824.
[4] H. Xu, H. Li, J. Xia, S. Yin, Z. Luo, L. Liu, L. Xu, ACS Appl. Mater. Interfaces 3 (2010) 22–29.
[5] Y. Xu, H. Xu, J. Yan, H. Li, L. Huang, Q. Zhang, C. Huang, H. Wan, Phys. Chem. Chem. Phys. 15 (2013) 5821–5830.
[6] Y. Liu, L. Fang, H. Lu, Y. Li, C. Hu, H. Yu, Appl. Catal. B Environ. 115–116 (2012) 245–252.
[7] J. Song, J. Roh, I. Lee, J. Jang, Dalton Trans. 42 (2013) 13897–13904.
[8] G.A. Bowmaker, J.V. Hanna, B.W. Skelton, A.H. White, Dalton Trans. 41 (2012) 5409–5417.
[9] Y. Bi, S. Ouyang, J. Cao, J. Ye, Phys. Chem. Chem. Phys. 13 (2011) 10071–10075.
[10] Z. Ji, X. Shen, J. Yang, Y. Xu, G. Zhu, K. Chen, Eur. J. Inorg. Chem. 2013 (2013) 6119–6125.
[11] H. Zhang, X. Fan, X. Quan, S. Chen, H. Yu, Environ. Sci. Technol. 45 (2011) 5731–5736.
[12] M. Zhu, P. Chen, M. Liu, ACS Nano 5 (2011) 4529–4536.
[13] X. Yang, H. Cui, Y. Li, J. Qin, R. Zhang, H. Tang, ACS Catal. 3 (2013) 363–369.
[14] C. Dong, K. Wu, X. Wei, X. Li, L. Liu, T. Ding, J. Wang, Y. Ye, CrystEngComm 16 (2014) 730–736.
[15] K. Zhang, N. Heo, X. Shi, J. Park, J. Phys. Chem. C 117 (2013) 24023–24032.
[16] S. William, Jr. Hummers, R.E. Offeman, J. Am. Chem. Soc. 80 (1958) 1339.
[17] H. Zhang, X. Lv, Y. Li, Y. Wang, J. Li, ACS Nano 4 (2009) 380–386.
[18] H. An, B. Zhu, J. Li, J. Zhou, S. Wang, S. Zhang, S. Wu, W. Huang, J. Phys. Chem. C 112 (2008) 18772–18775.
[19] L. Liu, J. Liu, D. Sun, Catal. Sci. Technol. 2 (2012) 2525–2532.
[20] L. Ye, J. Fu, Z. Xu, R. Yuan, Z. Li, ACS Appl. Mater. Interfaces 6 (2014) 3483–3490.
[21] D.S. Sagatys, G. Smith, R. Bott, D. Lynch, Polyhedron 12 (1993) 709–713.
[22] Y. Ao, P. Wang, C. Wang, J. Hou, J. Qian, Appl. Surf. Sci. 271 (2013) 265–270.
[23] P. Wang, B. Huang, X. Qin, X. Zhang, Y. Dai, J. Wei, M. Whangbo, Angew. Chem. Int. Ed. 47 (2008) 7931–7933.
[24] P. Wang, B. Huang, Q. Zhang, X. Zhang, X. Qin, Y. Dai, J. Zhan, J. Yu, H. Liu, Z. Lou, Chem. Eur. J. 16 (2010) 10042–10047.
[25] H. Yu, L. Liu, X. Wang, P. Wang, J. Yu, Y. Wang, Dalton Trans. 41 (2012) 10405–10411.
[26] T. Wu, G. Liu, J. Zhao, H. Hidaka, N. Serpone, J. Phys. Chem. B 102 (1998) 5845–5851.